ACS Photonics

Letter

Cite This: ACS Photonics 2017, 4, 2676-2680

pubs.acs.org/journal/apchd5

Nanoscale Laser Terahertz Emission Microscopy

Pernille Klarskov,*[,†,‡] Hyewon Kim,[§] Vicki L. Colvin,[†,§] and Daniel M. Mittleman*[,†]

[†]School of Engineering and [§]Department of Chemistry, Brown University, Providence, Rhode Island 02912, United States

[‡]DTU Fotonik - Department of Photonics Engineering, Technical University of Denmark, Dk-2800 Kongens Lyngby, Denmark

Supporting Information

ABSTRACT: Laser terahertz emission microscopy (LTEM) has become a powerful tool for studying ultrafast dynamics and local fields in many different types of materials. This technique, which relies on acceleration of charge carriers in a material upon femtosecond excitation, can provide insight into the physics of charge transport, built-in fields, grain boundaries or surface states. We describe a new implementation of LTEM with a spatial resolution in the nanoscale regime based on a scattering-type near-field tip-based approach. We observe a spectral reshaping of the signal compared to conventional LTEM, which is analyzed using a resonant antenna model. Our experimental and computational results clarify the importance of the mechanisms for both the plasmonic in-coupling of the near-infrared pulses into the near field and the out-coupling of the generated terahertz pulses. We demonstrate a tip-size-limited spatial resolution of ∼20 nm by imaging a gold nanorod using terahertz emission from the underlying substrate. This work enables for the first time the possibility of performing LTEM measurements on individual nanostructures.

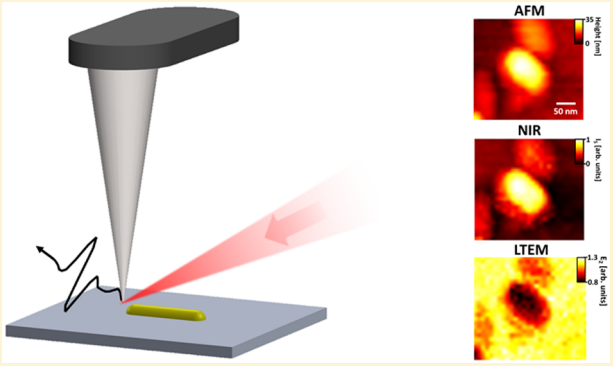

KEYWORDS: *terahertz emission microscopy, near-field imaging, apertureless NSOM, nonlinear optics*

In recent years, terahertz (THz) spectroscopic techniques have evolved into powerful tools for probing ultrafast dynamics in condensed matter systems, offering new opportunities for time-resolved measurements.[1] Especially when combined with subwavelength imaging, THz techniques, such as near-field pump−probe[2,3] or THz-assisted STM[4−6] can reveal new aspects of spatiotemporal dynamics. One versatile spectroscopic imaging method is laser THz emission microscopy (LTEM), which uses THz pulses emitted by a sample as diagnostics of charge or polarization dynamics. This technique relies on the generation and acceleration of charge carriers in a material upon femtosecond illumination. LTEM has been used for imaging[7,8] and spectroscopy[9,10] on a wide range of materials. Compared to other standard tools for terahertz spectroscopy, LTEM typically achieves superior spatial resolution, as it is limited by the focusing of the incident optical field, instead of the emitted terahertz field.[11] However, this spatial resolution is inadequate for studying individual nanostructures.

Here, we describe a technique to improve the resolution of LTEM by 3 orders of magnitude into the nanoscale regime using a scattering-type near-field microscope. Scattering-type (or apertureless) scanning near-field optical microscopy (s-SNOM)[12] has revolutionized the world of near-field imaging and spectroscopy. The sharp metal tip can serve not only to confine an incident optical field in a subwavelength region for nanoscale imaging and spectroscopy,[13−15] but also can induce an optical nonlinearity in this small sample volume. Recent examples of the latter include tip-enhanced Raman scattering[16] and tip-induced harmonic generation.[17] These tip-based techniques have also been adopted by THz researchers,[18,19] enabling THz imaging[13] and time-resolved THz spectroscopy[2] with resolution in the 10 nm range. Yet, LTEM has so far not been implemented in conjunction with s-SNOM.

In our experiment, we generate THz radiation by illuminating a tapered metal tip, near a surface, with near-infrared (NIR) femtosecond (fs) pulses. This s-SNOM situation is somewhat more complex than other nonlinear tip-based techniques due to the dramatic mismatch between the wavelengths of the incident (λ = 820 nm) and generated ($\lambda \sim$ hundreds of μm) fields. For example, our results demonstrate that both the plasmonic field enhancement of the NIR field near the illuminated metal tip[17] and the coupling of this tip antenna to the optically induced THz dipole[18,20] play important roles. As a result, unlike most other s-SNOM experiments, the decay of an approach curve is not necessarily indicative of the achievable spatial resolution. We elucidate the physics of this nonlinear optical interaction and demonstrate a spatial resolution of ∼20 nm by imaging a single nanoparticle, which enables new and exciting possibilities for terahertz spectroscopy on the nanoscale.

Received: August 4, 2017
Published: October 12, 2017

DOI: 10.1021/acsphotonics.7b00870
ACS Photonics 2017, 4, 2676−2680

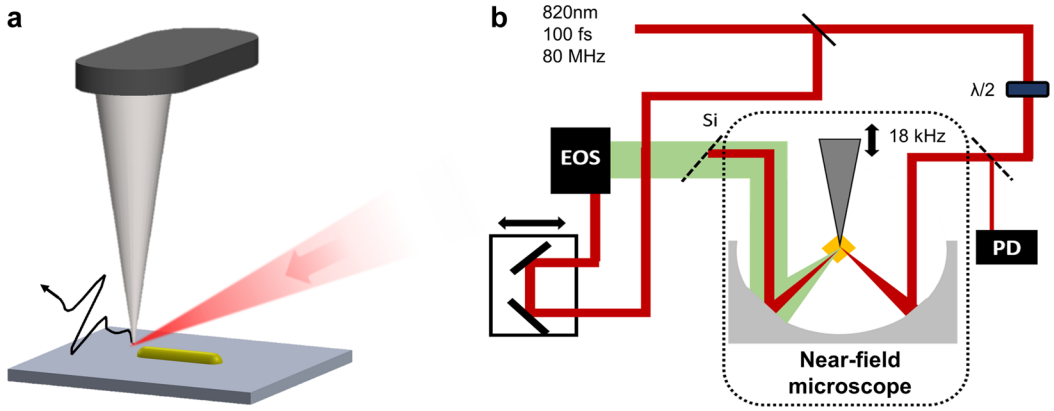

Figure 1. Experimental setup for nanoscale LTEM. (a) An illustration of the nanoscale LTEM experiment where an NIR beam (820 nm) is coupled to a sharp AFM tip, inducing THz radiation from a semiconductor substrate. (b) Schematic of the nanoscale LTEM setup where the backscattered near-field signal at 820 nm is measured on the right side of the microscope with a photodiode (PD) and the forward-scattered THz signal is measured by electro-optic sampling (EOS) on the left side.

Our experimental configuration is illustrated in Figure 1. We couple a fs laser beam (35 mW, 100 fs, 80 MHz repetition rate, 820 nm) to a commercial atomic force microscope (AFM), which operates in tapping mode with an 80 μm long Pt coated probe, tapering to a diameter of approximately 20 nm. We use the AFM in tapping mode, so that the tip is held at a constant average height above the sample, following the topography. The incident polarization is controlled by a half-wave plate and is set vertical for optimum NIR near-field coupling. The sample is a featureless wafer of *p*-doped (100) InAs (doping concentration ~10^{16} cm^{-3}), which is a well-known and efficient THz emitter[21] due to the photo-Dember effect.[22] We detect the backscattered NIR signal using a photodiode. By referencing the lock-in amplifier to a harmonic of the cantilever tapping frequency, we obtain pure near-field information from this backscattered optical signal.[12] We detect the forward-scattered THz signal by conventional electro-optic sampling in a 2 mm thick ZnTe, using a Si wafer to block forward-scattered NIR light (see Figure 1b). As with the NIR near-field signal, the THz signal is also detected by referencing the lock-in amplifier to either the fundamental or to a harmonic of the tapping frequency. Alternatively, we can simply chop the input NIR beam, and detect the customary LTEM signal generated from a larger region (a few μm diameter) on the sample surface. Simultaneously with the near-field NIR and THz data, we also record AFM topography.

Figure 2 shows a comparison of the customary LTEM signal (generated from a larger area) and a tip-locked signal (detected using a lock-in referenced to the tapping frequency). The relative signal amplitudes are difficult to compare; however, their spectral widths provide an important insight into the mechanism for THz generation and radiation into the far field. As it is clear from the widths of the pulses in the time domain, the THz bandwidth is similar for these two signals. This is quite distinct from the results of earlier broadband THz s-SNOM experiments, where a spectral narrowing was observed since the near-field probe behaved as an antenna, leading to a spectral filtering and narrowing of the scattered THz spectrum by about a factor of 3.[18,20] To quantify whether the AFM probe acts as an antenna in our experiment, we plot in Figure 2b the ratio of the two amplitude spectra of the waveforms in Figure 2a (black curve). We observe a slight shift of the spectrum toward higher frequencies. To explain this we include a simple model calculation (blue curve) based on a purely resistive antenna

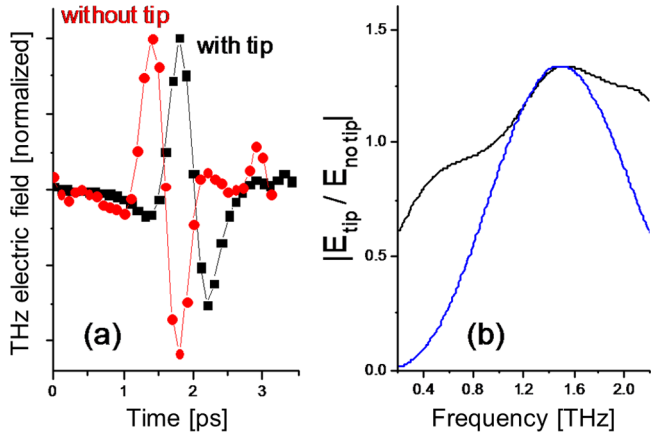

Figure 2. Comparison of conventional LTEM and tip-locked THz signals. (a) THz waveforms measured by conventional LTEM (shown in red, where the signal originates from the entire area illuminated by the incident NIR pulse) and by tip-coupled LTEM (shown in black, where the signal is measured by locking to the second harmonic of the AFM tapping frequency). These two time-domain waveforms, which have been normalized to unity height to facilitate comparison, have very similar shape and duration, indicating very similar spectral content. The relative temporal shift of the waveforms is a measurement artifact, and is therefore not significant. (b) Experimental (black curve) and computed (blue curve) ratio of the electric field amplitudes of the two waveforms in (a).

coupling for the tip-locked signal (see Supporting Information). Using an antenna length of 80 μm (corresponding to the length of our AFM probe tip), this model predicts the location and approximate width of the weak peak at 1.5 THz observed in the measured spectral ratio. This relatively small but repeatable antenna effect emphasizes the role of the coupling of the generated THz dipole to the AFM probe.[23]

To further elucidate the mechanism for signal generation, we measure the approach curve, simultaneously for both the NIR and THz signals, by withdrawing the tip from the surface and measuring the signal decay as a function of tip−sample separation (Figure 3a). In s-SNOM experiments, approach curves are conventionally used to define the spatial confinement of the NIR near field,[23] and hence provide information about the expected lateral image resolution. As expected for s-SNOM approach curves, we observe an exponential decay of

DOI: 10.1021/acsphotonics.7b00870
ACS Photonics 2017, 4, 2676−2680

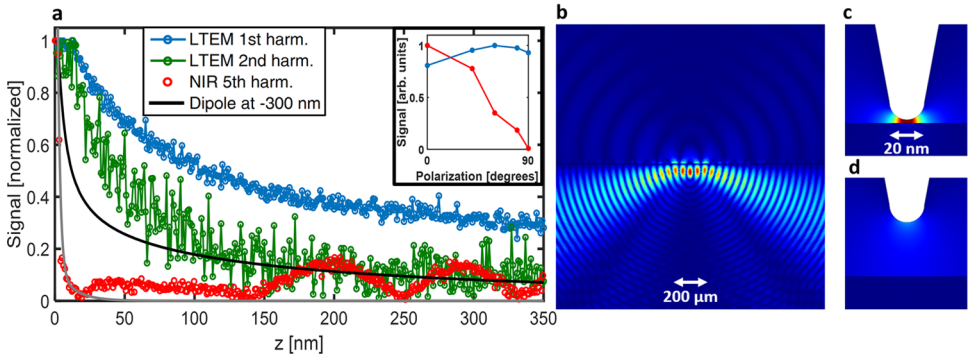

Figure 3. Coupling of THz dipole from substrate to AFM tip. (a) Approach curves measured for the 1st and 2nd harmonic tip-locked LTEM signal together with the 5th harmonic NIR near-field signal, all measured above the bare InAs substrate. The black curve is extracted from numerical simulations of a THz dipole in the substrate and its coupling to a nanoscale metal tip held above the surface, as described in the text. The gray curve is an exponential fit to the NIR data for $z < 20$ nm. (b) Illustrative example of the simulation of a dipole in the substrate radiating at 1 THz. (c) Simulation illustrating the coupling of this THz dipole to the metal tip when the tip is displaced 5 nm and (d) 35 nm from the surface. In (b), the scale bar is 200 μm. In (c), it is 20 nm (the scale is the same for (c) and (d)).

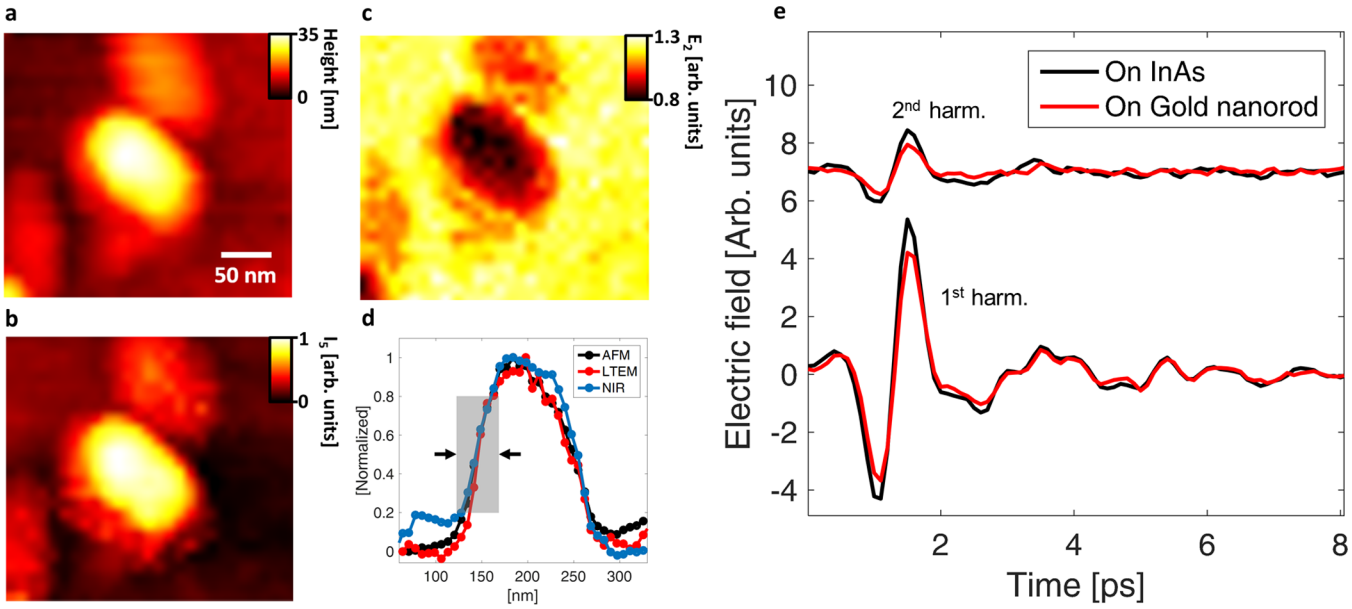

Figure 4. Imaging of gold nanorods. (a) AFM topography image, showing that the nanorod has a height of ~35 nm. (b) An optical near-field image formed using the backscattered 820 nm light (locked to the fifth harmonic of the tip oscillation). This signal is significantly stronger from the gold nanorod than from the substrate as anticipated, because of the much higher dielectric constant of gold. (c) An LTEM image formed using the peak THz field (locked to the second harmonic of the tip oscillation). (d) Line scans along the axis of the gold nanorod from the three images shown in (a), (b), and (c) (AFM in black, LTEM in red, NIR in blue), all normalized to unity height to facilitate comparison of the spatial resolution. The gray box indicates the 20–80% rise of these line scans, which are 31, 33, and 26 nm for the AFM, NIR, and LTEM images, respectively. (e) THz waveforms measured from the 1st and 2nd harmonic LTEM signal when the tip is above the InAs substrate (black) and above the gold nanorod (red).

the NIR near-field when the tip–sample distance is less than 20 nm (red points in Figure 3a). The oscillations in this signal at $z > 150$ nm are due to standing waves from reflections between the sample and the AFM cantilever.[23,24] However, the THz signal exhibit a much slower decay, even for the signal measured at the second harmonic of the tapping frequency (green curve), for which the delocalized background component is essentially absent.

This slower decay of the THz approach curve seems to suggest that the spatial localization and lateral resolution of the LTEM signal is not as small as the 20 nm AFM tip. However, the nonlinear LTEM process is fundamentally different from s-SNOM because the input and output waves here are of very dissimilar wavelengths. The LTEM signal obtained by lock-in detection to the tip oscillation can originate from the following two processes: first, the tip-induced THz signal which is generated only when the semiconducting substrate is in direct contact with the NIR near-field which is confined under the sharp metal AFM tip. Since the substrate is spatially uniform, the carriers which are photoexcited by the NIR near-field are expected to diffuse hundreds of nanometers in to the substrate,[25] creating a THz dipole that is not restricted in lateral size despite originating from a subwavelength volume. Second, we note that that the area illuminated by the focused laser pulse is macroscopic (i.e., limited by the optical wavelength and the far-field focusing optics). This illumination induces a large THz dipole in the InAs which is, however, still smaller than any wavelength in the bandwidth of the generated

DOI: 10.1021/acsphotonics.7b00870
ACS Photonics 2017, 4, 2676–2680

THz pulse. This macroscopic THz dipole can be subsequently probed and out-coupled by the oscillating AFM tip. To clarify this two-step mechanism, we have performed numerical simulations using a frequency domain finite-element method (FD-FEM) solver to study the coupling of a THz dipole just below the surface of a dielectric to a nearby tapered metal tip. Here, a dipole oscillating at 1 THz is located 300 nm below the substrate surface[25] as illustrated in Figure 3b, which shows a simulation of the radiating THz dipole without the tip. We then include the tip in the simulation, and extract the strength of the electric field at a distance of 10 nm from the center of the tip (which has a 20 nm diameter), as a function of tip−sample separation. This result is shown in Figure 3a (black curve). The decay of this tip-coupled THz signal with the tip−sample separation is significantly slower than that of the measured NIR near-field signal, similar to what is observed in the experimental THz approach curve, even though the out-coupled THz field is still strongly confined to a ∼20 nm region very close to the metal tip (e.g., Figure 3c,d). This result suggests that the localized out-coupling of a macroscopic THz dipole plays a significant role in the measured tip-locked LTEM signal. Yet, since the out-coupled field is still strongly localized by the probe tip, this slow decay of the THz approach curve is not indicative of a lower spatial resolution in our measurements, unlike in other s-SNOM experiments.[2,17] To confirm this hypothesis we perform an additional experiment where we measure the tip-locked LTEM and NIR near-field signal's dependence on the polarization of the incident NIR beam (see inset in Figure 3a). As expected, the NIR near-field signal vanishes when the polarization is rotated from vertical (parallel to the AFM tip) to horizontal. In contrast, the LTEM signal barely changes at all. This result demonstrates that the out-coupling of a macroscopic THz dipole, coupled to the tip antenna, is responsible for the detected LTEM signal.

In order to verify the image resolution, we prepare a solution of gold nanorods with a strong absorption in the visible and NIR, using standard methods.[26] This sample was drop-cast onto the p-InAs wafer and dried. Subsequently, we image small regions of this decorated wafer using AFM and the NIR near-field, as well as the peak of the emitted THz field. Representative images of a particular nanorod are shown in Figure 4 (see Supporting Information for additional images). The measured LTEM image (Figure 4c) shows similar spatial contrast to the AFM topography (Figure 4a) and optical near-field (Figure 4b) images; however, the contrast is inverted, with a larger THz peak field when the tip is above the bare substrate and slightly smaller signal when above the gold nanorod. Figure 4d shows line cuts through these three images, indicating that all three have similar spatial resolution. Indeed, the edges are slightly sharper in the LTEM image which may be due to the nonlinear nature of the THz generation process. To quantify this we measure the 20−80% rise distance (indicated by the gray box in Figure 4d) to be 31, 33, and 26 nm for the AFM, NIR, and LTEM images, respectively.

To illustrate the image contrast, Figure 4e shows representative THz waveforms measured when the tip is above the InAs and the gold nanorod. The fact that only a small decrease in both the first and second harmonic signal is observed when the AFM tip is located above the gold nanorod may indicate a plasmonic coupling of the near-field signal to the substrate or of the THz dipole to the nanorod, mediated by the metal nanorod's localized plasmon resonance (see Supporting Information). In addition, the skin depth of gold at 1 THz is about 75 nm which is about twice as large as the thickness of the nanorods. Therefore, screening of the emitted THz field by the superimposed gold rod may also play a role in the diminished signal. Future experiments with a tunable incident pulse will clarify this contrast mechanism.

In summary, we have demonstrated laser THz emission microscopy with a spatial resolution of ∼20 nm, limited by the size of our AFM tip. We have demonstrated that, unlike optical near-field images, the decay of the approach curve in this nonlinear process does not necessarily give a good indication of the lateral spatial resolution, and furthermore that the LTEM signal is roughly independent of the incident light's polarization. This is in marked contrast to a conventional s-SNOM experiment in which a vertical (aligned with the AFM tip) polarization is required. We have also clarified the role of antenna effects in transducing the signal into the far field. Our results open up many new possibilities for emission spectroscopy of individual nanostructures.

■ ASSOCIATED CONTENT

Supporting Information

The Supporting Information is available free of charge on the ACS Publications website at DOI: 10.1021/acsphotonics.7b00870.

Properties of gold nanorods, additional LTEM images taken at harmonics of the AFM tapping frequency, and antenna transfer function calculation (PDF).

■ AUTHOR INFORMATION

Corresponding Authors

*E-mail: pernille_klarskov@brown.edu.
*E-mail: daniel_mittleman@brown.edu.

ORCID

Daniel M. Mittleman: 0000-0003-4277-7419

Author Contributions

P.K. performed the experiments, simulations, and data analysis. D.M.M. developed the theoretical model. H.K. and V.L.C. synthesized the gold nanorods. P.K. and D.M.M. wrote and reviewed the manuscript.

Notes

The authors declare no competing financial interest.

■ ACKNOWLEDGMENTS

We acknowledge financial support from the Danish Council for Independent Research (FTP Project HI-TEM) and from the U.S. National Science Foundation (NSF). We also acknowledge funding support from NNSA's Kansas City National Security Campus operated by Honeywell FM&T under prime contract DE-NA0002839. We also gratefully acknowledge Dr. Frank Hegmann and Dr. Peter Uhd Jepsen for valuable discussions.

■ REFERENCES

(1) Kampfrath, T.; Tanaka, K.; Nelson, K. A. Resonant and nonresonant control over matter and light by intense terahertz transients. *Nat. Photonics* **2013**, *7*, 680−690.

(2) Eisele, M.; Cocker, T. L.; Huber, M. A.; Plankl, M.; Viti, L.; Ercolani, D.; Sorba, L.; Vitiello, M. S.; Huber, R. Ultrafast multi-terahertz nano-spectroscopy with sub-cycle temporal resolution. *Nat. Photonics* **2014**, *8*, 841−845.

(3) Huber, M. A.; Mooshammer, F.; Plankl, M.; Viti, L.; Sandner, F.; Kastner, L. Z.; Frank, T.; Fabian, J.; Vitiello, M. S.; Cocker, T. L.;

DOI: 10.1021/acsphotonics.7b00870
ACS Photonics 2017, 4, 2676−2680

Huber, R. Femtosecond photo-switching of interface polaritons in black phosphorus heterostructures. *Nat. Nanotechnol.* **2016**, *12*, 207−211.
(4) Cocker, T. L.; Jelic, V.; Gupta, M.; Molesky, S. J.; Burgess, J. A. J.; Reyes, G. D. L.; Titova, L. V.; Tsui, Y. Y.; Freeman, M. R.; Hegmann, F. A. An ultrafast terahertz scanning tunnelling microscope. *Nat. Photonics* **2013**, *7*, 620−625.
(5) Cocker, T. L.; Peller, D.; Yu, P.; Repp, J.; Huber, R. Tracking the ultrafast motion of a single molecule by femtosecond orbital imaging. *Nature* **2016**, *539*, 263−267.
(6) Jelic, V.; Iwaszczuk, K.; Nguyen, P. H.; Rathje, C.; Hornig, G. J.; Sharum, H. M.; Hoffman, J. R.; Freeman, M. R.; Hegmann, F. A. Ultrafast terahertz control of extreme tunnel currents through single atoms on a silicon surface. *Nat. Phys.* **2017**, *13*, 591−598.
(7) Kiwa, T.; Tonouchi, M.; Yamashita, M.; Kawase, K. Laser terahertz-emission microscope for inspecting electrical faults in integrated circuits. *Opt. Lett.* **2003**, *28*, 2058−2060.
(8) Tonouchi, M.; Yamashita, M.; Hangyo, M. Terahertz radiation imaging of supercurrent distribution in vortex-penetrated $YBa_2Cu_3O_{7-\delta}$ thin film strips. *J. Appl. Phys.* **2000**, *87*, 7366−7375.
(9) Nakanishi, H.; Fujiwara, S.; Takayama, K.; Kawayama, I.; Murakami, H.; Tonouchi, M. Imaging of a polycrystalline silicon solar cell using a laser terahertz emission microscope. *Appl. Phys. Express* **2012**, *5*, 112301.
(10) Sakai, Y.; Kawayama, I.; Nakanishi, H.; Tonouchi, M. Polarization imaging of imperfect m-plane GaN surfaces. *APL Photon.* **2017**, *2*, 041304.
(11) Murakami, H.; Serita, K.; Maekawa, Y.; Fujiwara, S.; Matsuda, E.; Kim, S.; Kawayama, I.; Tonouchi, M. Scanning laser THz imaging system. *J. Phys. D: Appl. Phys.* **2014**, *47*, 374007.
(12) Hillenbrand, R.; Taubner, T.; Keilmann, F. Phonon-enhanced light matter interaction at the nanometre scale. *Nature* **2002**, *418*, 159−162.
(13) Huber, A. J.; Keilmann, F.; Wittborn, J.; Aizpurua, J.; Hillenbrand, R. Terahertz near-field nanoscopy of mobile carriers in single semiconductor nanodevices. *Nano Lett.* **2008**, *8*, 3766−3770.
(14) Fei, Z.; Andreev, G. O.; Bao, W.; Zhang, L. M.; A, S. M.; Wang, C.; Stewart, M. K.; Zhao, Z.; Dominguez, G.; Thiemens, M.; Fogler, M. M.; Tauber, M. J.; Castro-Neto, A. H.; Lau, C. N.; Keilmann, F.; Basov, D. N. Infrared nanoscopy of Dirac plasmons at the graphene−SiO_2 interface. *Nano Lett.* **2011**, *11* (11), 4701−4705.
(15) Chen, J.; Badioli, M.; Alonso-Gonzalez, P.; Thongrattanasiri, S.; Huth, F.; Osmond, J.; Spasenovic, M.; Centeno, A.; Pesquera, A.; Godignon, P.; Elorza, A. Z.; Camara, N.; Garcia de Abajo, F. J.; Hillenbrand, R.; Koppens, F. H. Optical nano-imaging of gate-tunable graphene plasmons. *Nature* **2012**, *487*, 77−81.
(16) Stöckle, R. M.; Suh, Y. D.; Deckert, V.; Zenobi, R. Nanoscale chemical analysis by tip-enhanced Raman spectroscopy. *Chem. Phys. Lett.* **2000**, *318*, 131−136.
(17) Atkin, J. M.; Berweger, S.; Jones, A. C.; Raschke, M. B. Nano-optical imaging and spectroscopy of order, phases, and domains in complex solids. *Adv. Phys.* **2012**, *61*, 745−842.
(18) Wang, K.; Mittleman, D. M.; van der Valk, N. C. J.; Planken, P. C. M. Antenna effects in terahertz apertureless near-field optical microscopy. *Appl. Phys. Lett.* **2004**, *85*, 2715−2717.
(19) Planken, P. C. M.; van Rijmenam, C. E. W. M.; Schouten, R. N. Opto-electronic pulsed THz systems. *Semicond. Sci. Technol.* **2005**, *20*, S121−S127.
(20) Chen, H.-T.; Kraatz, S.; Cho, G. C.; Kersting, R. Identification of a resonant imaging process in apertureless near-field microscopy. *Phys. Rev. Lett.* **2004**, *93*, 267401.
(21) Gu, P.; Tani, M.; Kono, S.; Sakai, K.; Zhang, X. C. Study of terahertz radiation from InAs and InSb. *J. Appl. Phys.* **2002**, *91*, 5533−5537.
(22) Reklaitis, A. Terahertz emission from InAs induced by photo-Dember effect: Hydrodynamic analysis and Monte Carlo simulations. *J. Appl. Phys.* **2010**, *108*, 053102.
(23) Hecht, B.; Bielefeldt, H.; Inouye, Y.; Pohl, D. W.; Novotny, L. Facts and artifacts in near-field optical microscopy. *J. Appl. Phys.* **1997**, *81*, 2492−2498.
(24) Wang, K.; Barkan, A.; Mittleman, D. M. Propagation effects in apertureless near-field optical antennas. *Appl. Phys. Lett.* **2004**, *84*, 305−307.
(25) Polyakov, V. M.; Schwierz, F. Influence of band structure and intrinsic carrier concentration on the THz surface emission from InN and InAs. *Semicond. Sci. Technol.* **2007**, *22*, 1016−1020.
(26) Ye, X.; Zheng, C.; Chen, J.; Gao, Y.; Murray, C. B. Using binary surfactant mixtures to simultaneously improve the dimensional tunability and monodispersity in the seeded growth of gold nanorods. *Nano Lett.* **2013**, *13*, 765−771.

DOI: 10.1021/acsphotonics.7b00870
ACS Photonics 2017, 4, 2676−2680